Energy & Environmental Science

PAPER

View Article Online
View Journal | View Issue

Cite this: *Energy Environ. Sci.*, 2018, **11**, 3443

Enhanced photothermal reduction of gaseous CO_2 over silicon photonic crystal supported ruthenium at ambient temperature†

Paul G. O'Brien,[a] Kulbir K. Ghuman,[b] Abdinoor A. Jelle,[c] Amit Sandhel,[d] Thomas E. Wood,[e] Joel Y. Y. Loh,[f] Jia Jia,[d] Doug Perovic,[c] Chandra Veer Singh,[c] Nazir P. Kherani,[cf] Charles A. Mims[e] and Geoffrey A. Ozin*[d]

Received 12th August 2018,
Accepted 9th October 2018

DOI: 10.1039/c8ee02347f

rsc.li/ees

Solar-driven CO_2 hydrogenation can provide a renewable source of fuels and reduce greenhouse gas emissions if operated at industrial scales. Herein we investigate the photomethanation (light-driven Sabatier reaction) rates over Ru films sputtered onto silica opal (Ru/SiO_2) and inverted silicon opal photonic crystal (Ru/i-Si-o) supports at ambient temperature under solar-simulated radiation as a function of incident light intensity. Photomethanation rates over both the Ru/SiO_2 and Ru/i-Si-o catalysts increase significantly with increasing light intensity, and rates as large as 2.8 mmol g^{-1} h^{-1} are achieved over the Ru/i-Si-o catalyst. Furthermore, the quantum efficiency of the photomethanation reaction is almost three times larger when measured over the Ru/i-Si-o catalyst as compared to the Ru/SiO_2 catalyst. The large photomethanation rates over the Ru/i-Si-o catalyst are attributed to its exceptional light-harvesting properties. Moreover, we perform DFT analysis to investigate the potential role of photo-induced charges on the Ru surface. The results from the simulation indicate that charged Ru surfaces can destabilize adsorbed CO_2 molecules and adsorb and dissociate H_2 such that it can readily react with CO_2, thereby accelerating the Sabatier reaction.

Broader context

Methane has a high H : C ratio and gross heating value and is one of the cleanest fossil fuel energy sources. However, CH_4 combustion still produces CO_2 emissions. Also, CH_4 is a more potent greenhouse gas than CO_2 and escapes to the atmosphere during modern day extraction processes. As an alternative method of acquiring CH_4, CO_2 hydrogenation can be driven with solar energy using hydrogen generated from renewable or excess energy sources. If ran at industrial scales, this represents an important reaction that can be used to close the carbon cycle by producing CH_4 that can be readily stored in existing natural gas pipelines. Herein we show that gas phase CO_2 at ambient temperatures can be converted to methane over Ru-films coated onto photonic crystal supports that are subjected to highly concentrated solar-simulated radiation. The reaction occurs *via* a photothermal effect, whereby high-energy high-intensity light heats the Ru film at the photonic crystal surface. Furthermore, DFT analysis shows that photoinduced charges on the surface of the Ru film can accelerate photothermal reaction rates by activating adsorbed reactants. The results bode well for the design of a large-scale solar-driven CO_2 recycling process that can readily be integrated with the existing energy infrastructure.

Introduction

Important modern day environmental challenges are climate change and ocean acidification caused by increasing levels of anthropogenic CO_2 emissions, primarily brought about by burning fossil fuel energy sources.[1–6] One potential solution to simultaneously mitigate the effects of CO_2 emissions and provide sustainable energy is to utilize CO_2 as a feedstock chemical that can be converted to fuels using solar energy.[7–15] In this context, gas phase CO_2 reduction to fuels such as methane, which can be readily transported in existing natural gas pipelines, has garnered interest on account of its potential for large-scale production.[16–19]

The Sabatier reaction ($CO_2 + 4H_2 \rightarrow CH_4 + 2H_2O$) is most commonly driven over Ru- and Ni-based catalysts, although other

[a] *Department of Mechanical Engineering, Lassonde School of Engineering York University, 4700 Keele Street, Toronto, Ontario, M3J 1P3, Canada*
[b] *International Institute for Carbon-Neutral Energy Research, Kyushu University, 744 Motooka, Nishi-ku, Fukuoka, 819-0395, Japan*
[c] *Department of Materials Science and Engineering, University of Toronto, 184 College Street, Toronto, Ontario, M5S 3E4, Canada*
[d] *Department of Chemistry, University of Toronto, 80 St. George St., Toronto, Ontario, M5S 3H6, Canada. E-mail: gozin@chem.utoronto.ca*
[e] *Department of Chemical Engineering and Applied Chemistry, University of Toronto, 200 College St., Toronto, Ontario, M5S 3E5, Canada*
[f] *Department of Electrical and Computer Engineering, University of Toronto, 10 King's College Road, Toronto, Ontario, M5S 3G4, Canada*

† Electronic supplementary information (ESI) available. See DOI: 10.1039/c8ee02347f

catalysts have been investigated.[20–24] The potential to drive the Sabatier reaction with solar irradiance has been investigated over semiconductor, layer-double hydroxide, and supported metallic catalysts.[25–27] Furthermore, photomethanation experiments over various catalysts have been performed to investigate whether the photocatalyst activity is of a photothermal nature, wherein photo-excited charge carriers completely thermalize to heat energy which activates the reaction, or if there is a photochemical contribution to the reaction, whereby photogenerated charge carriers induce changes in the chemical bonds of reactant species or chemical intermediates.[28–31] For example, Sastre *et al.* reported the complete photochemical reduction of CO_2 to CH_4 over Ni/silica-alumina and proposed that photo-excited charges promote the formation of active Ni–H species that accelerate the reaction.[32]

In previous work we achieved gas-phase photomethanation rates of 1 mmol g_{cat}^{-1} h^{-1} over Ru sputtered on silicon nanowires (black silicon) subjected to solar-simulated radiation.[33] These high photomethanation rates were attributed to enhanced light absorption in the black silicon support over the broad solar spectrum, including visible and near-infrared photons. We also investigated gaseous CO_2 photoreduction over hydroxylated indium oxide nanoparticles coated onto black silicon supports and the results showed this hybrid photocatalyst used the UV portion of the solar-simulated irradiance to photochemically activate the reduction of CO_2 to CO while the visible and infrared portion of the incident solar irradiance provided photothermal energy which was instrumental for enabling the reaction.[34] Recently, we investigated the gas phase photomethanation of CO_2 with H_2 at ambient temperatures under high-intensity solar-simulated irradiation over RuO_2 nanocrystals on inverted silicon photonic crystal supports and the light absorption properties of these supports was found to enhance photomethanation rates.[35]

In this work we further investigate the ability to drive gas-phase CO_2 reduction at ambient temperatures using high intensity light by comparing photomethanation rates over Ru films sputtered on different photonic crystal (PC) supports. We investigate photomethanation rates over Ru films sputtered onto (1) an opaline PC support comprised of silica spheres (SiO_2-o) and (2) an inverted silicon opal PC support (i-Si-o). Furthermore, we perform density functional theory (DFT) analysis and the results suggest that photo-induced charges on the Ru surface could facilitate the formation of ruthenium–hydride bonds and accelerate the photomethanation reaction. PCs have been investigated as photocatalyst supports because they exhibit unique light-trapping properties, the slow photon effect, and can reduce recombination of photogenerated carriers by inhibiting spontaneous emission.[36–43] Furthermore, Si is an interesting choice of material for a photocatalyst support because, with a bandgap energy of 1.1 eV, it can absorb more than 80% of the solar irradiance.[44–46]

Results and discussion

Four samples were investigated in this study; bare SiO_2-o and i-Si-o PC supports and these supports with a 50 nm thick Ru film sputtered onto their surface (denoted as Ru/SiO_2-o and Ru/i-Si-o).

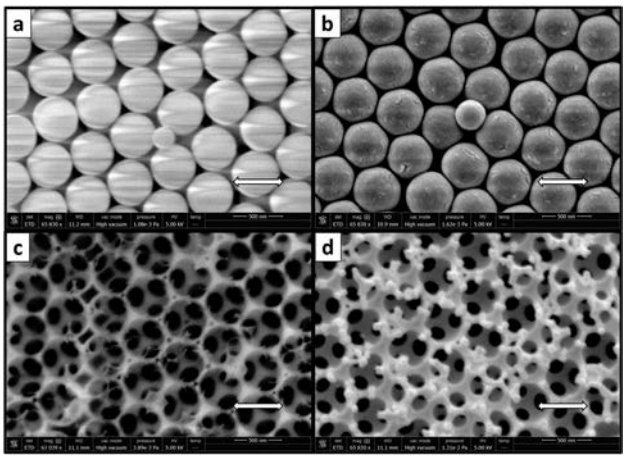

Fig. 1 SEM images of (a) a SiO_2-o film (b) a SiO_2-o film with 50 nm of Ru sputtered onto its surface (c) an i–Si-o film (d) an i-Si-o film with 50 nm of Ru sputtered onto its surface. The double sided arrows in each image represent a length scale of 500 nm. Note: the horizontal streaks in image (a) are due to charging of the insulating silica spheres in the SEM.

The methods used to fabricate the SiO_2-o and i-Si-o PCs have been described previously and are briefly summarized in the experimental section.[47] SEM images of the SiO_2-o, Ru/SiO_2-o, i-Si-o, and Ru/i-Si-o samples are shown in Fig. 1. To fabricate these samples RF magnetron sputtering was used to deposit a Ru film on the bare SiO_2-o and i-Si-o supports. The sputter deposition was stopped once 50 nm of Ru, as measured using an *in situ* thickness monitor, had been deposited. The sputtered Ru is deposited as a conformal film, with some cracks and surface texture, over the uppermost layer of the PC supports (Fig. S1, ESI†). The uppermost layers in the PC framework shadow the underlying layers, and it is expected that only the first few layers of the PC supports are coated with Ru.

The spectral reflectance, diffuse reflectance, and absorption of these samples are shown in Fig. 2a, b, and c, respectively. The spectral reflectance of the SiO_2-o support exhibits a peak at $\sim$1020 nm, which is consistent with the [111] stop-gap position in the direction normal to an opal PC film comprised of silica spheres with a diameter of 460 nm. The complete 3D photonic band-gap of the i-Si-o support resides in the spectral vicinity $\sim$800 nm, where a small reflection peak can be seen in Fig. 2a. The reflection peak from this 3D photonic band-gap is much less intense than that of the SiO_2-o PC due to absorption in the i-Si-o support. As shown in Fig. 2b, the diffuse reflectance of the bare supports is greater than their spectral reflection, showing these PCs are highly scattering in the visible and NIR spectral regions. The diffuse reflectance of the PC supports decreases after the Ru film is deposited on their surface. As shown in Fig. 2c, $\sim$90% of the light in the short-wavelength region ($\lambda < 500$ nm) incident onto the i-Si-o support is absorbed, and absorption decreases with increasing wavelength, however, Ru/i-Si-o absorbs $\sim$90% from 300 nm to 1200 nm. The SiO_2-o PC exhibits over 60% absorption from 700 nm to 950 nm. As silica is a transparent material, it can be noted that incident light within this spectral region is primarily absorbed by the silicon wafer that the SiO_2-o PC is deposited on. The Ru/SiO_2-o

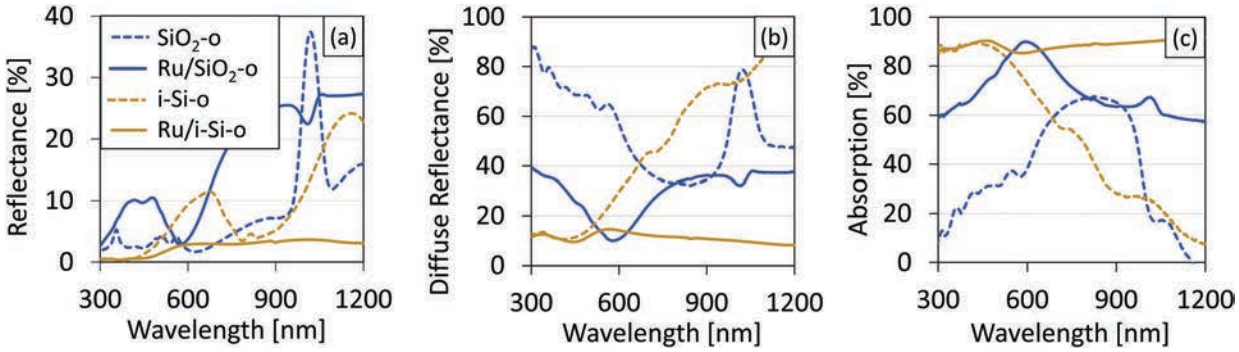

Fig. 2 The (a) reflectance, (b) diffuse reflectance, and (c) absorption of the SiO_2-o (blue lines) and i-Si-o films (brown lines) with (solid lines) and without (dashed lines) Ru deposited onto their surface.

sample absorbs ~70% on average of the incident light over the spectral range from 300 nm to 1200 nm.

A series of photomethanation rate measurements were performed on the SiO_2-o, Ru/SiO_2-o, i-Si-o, and Ru/i-Si-o samples under solar-simulated irradiation, produced from a 300 W Xe lamp, at varying light intensities with and without a 495 nm cut-off filter, and the results are plotted in Fig. 3a. For tests performed without a filter the maximum incident radiant power was 2470 mW cm^{-2} (or 24.7 Suns) and additional tests were performed at lower light intensities by increasing the distance between the Xe lamp and the reactor. For tests performed using the 495 nm cut-off filter the maximum incident radiant power was 1220 mW cm^{-2} (or 12.2 Suns). The relative spectral power distribution incident onto the samples for tests carried out with and without a 495 nm cut-off filter are shown in Fig. 3b. During the photomethanation rate measurements carried out under maximum incident radiant power the temperatures of the Ru/SiO_2-o and Ru/i-Si-o samples, measured with a thermocouple located on the rear side of the silicon wafer (the side that is opposite from the side with the photonic crystals and supported Ru), was observed to rise to ~150 °C (Fig. S2, ESI†). For comparison, methanation rates over all samples were also measured in the dark at 150 °C. The bare SiO_2-o and i-Si-o PC supports, tested under an irradiance of 2470 mW cm^{-2} and at 150 °C in the dark, did not yield any products. Moreover, XPS measurements confirmed that the Ru on the PC supports was in the metallic state, both before and after tests were performed (Fig. S3, ESI†).

The methanation rates in the dark at a temperature of 150 °C for the Ru/SiO_2-o and Ru/i-Si-o samples was observed to be 0.05 mmol g^{-1} h^{-1} and 0.36 mmol g^{-1} h^{-1}, respectively. The photomethanation rates measured over the Ru/SiO_2-o and Ru/i-Si-o samples under high intensity solar-simulated light was much greater than those measured in the dark at 150 °C. For experiments performed without the use of a filter, the photomethanation rate over the Ru/SiO_2 sample increased from 0.28 mmol g^{-1} h^{-1} to 0.79 mmol g^{-1} h^{-1} as the incident light intensity increased from 550 mW cm^{-2} to 2470 mW cm^{-2}. In comparison, the photomethanation rate over the Ru/i-Si-o

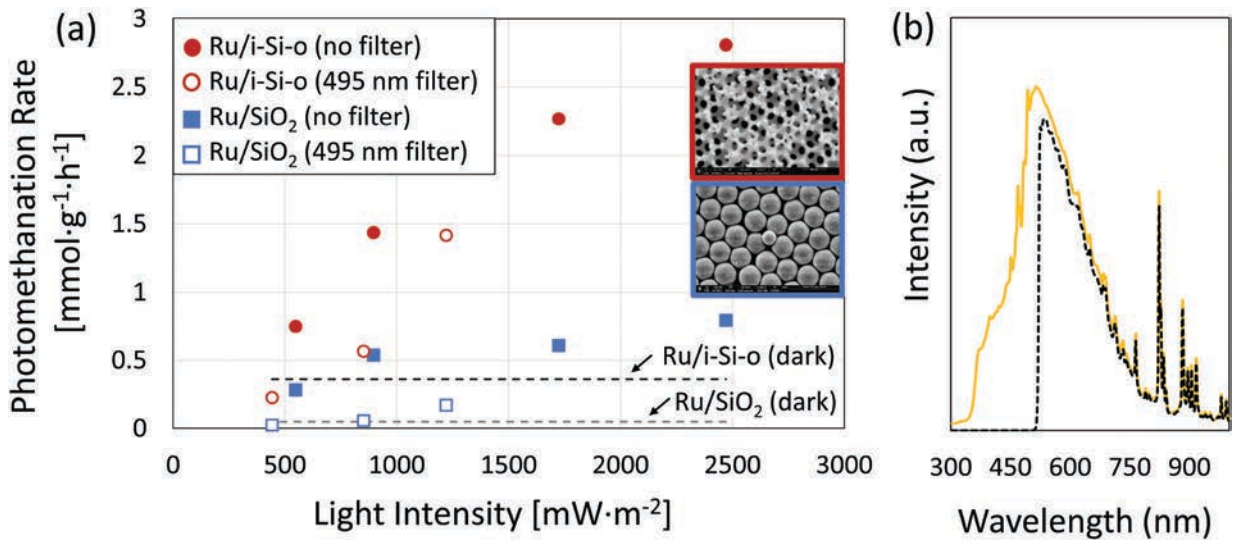

Fig. 3 (a) Photomethanation rates over Ru/i-Si-o and Ru/SiO_2-o as a function of incident light intensity; the solid and open shapes represent rates measured without a filter and with a 495 nm high-pass cut-off filter, respectively. The Methanation rates measured in the dark at 150 °C are shown as the dashed line for comparison. (b) The incident light spectra for tests performed without a filter and with a 495 nm high-pass cut-off filter. All rates were normalized to the total weight of the sputtered Ru (~1.2 mg).

sample increased from 0.75 mmol g^{-1} h^{-1} to 2.8 mmol g^{-1} h^{-1} as the incident light intensity increased from 550 mW cm^{-2} to 2470 mW cm^{-2}. This photomethanation rate of 2.8 mmol g^{-1} h^{-1} measured over the Ru/i-Si-o sample was the highest rate observed in this study. The photomethanation rates for the Ru/SiO_2-o and Ru/i-Si-o samples when tested using a 495 nm cut-off filter, at an intensity of 1220 mW cm^{-2}, was 0.17 mmol g^{-1} h^{-1} and 1.4 mmol g^{-1} h^{-1}, respectively. When tested using the 495 nm cut-off filter at the lower light intensity of 440 mW cm^{-2} the photomethanation rates over the Ru/SiO_2-o and Ru/i-Si-o samples was 0.03 mmol g^{-1} h^{-1} and 0.23 mmol g^{-1} h^{-1}, respectively, which is less than the rates observed at 150 °C in the dark for these samples. Furthermore, isotope tracing experiments using $^{13}CO_2$ as a reactant confirmed that the CH_4 produced in these reactions was $^{13}CH_4$ and therefore originated from $^{13}CO_2$ and not from adventitious carbon sources (Fig. S4, ESI†).

As shown in Fig. 3, both the Ru/SiO_2-o and Ru/i-Si-o samples exhibit significantly increased methanation rates under high-intensity solar-simulated radiation as compared to rates measured in the dark at 150 °C. The quantum efficiency (QE) for these photomethanation reactions was calculated as $QE = 8 \cdot N_{CH_4}/N_{ph} \cdot A$, where N_{CH_4} is the number of methane molecules produced, N_{ph} is the number of photons incident onto the catalyst and A is the absorption of the catalyst. The QE for the Ru/SiO_2-o and Ru/i-Si-o samples under solar-simulated light at an intensity of 2470 mW cm^{-2} is 1.0×10^{-4} and 3.1×10^{-4}, respectively. When tested using the 495 nm cut-off filter, with a light intensity of 1220 mW cm^{-2}, the QE for the Ru/SiO_2-o and Ru/i-Si-o samples is 3.5×10^{-5} and 2.6×10^{-4}, respectively. Thus, the QE of the photomethanation reaction over the Ru/i-Si-o sample is about three and seven times larger than the QE of the photomethanation reaction over the Ru/SiO_2-o sample when measured under light intensities of 2470 mW cm^{-2} and 1220 mW cm^{-2}, respectively. The larger photomethanation rates over Ru/i-Si-o compared to Ru/SiO_2-o may be caused by multiple mechanisms related to metal-support interactions, enhanced light absorption, localized heating and photo-induced charges.[48–50]

As shown in Fig. 2c, the average absorption in the Ru/i-Si-o sample is greater than that of the Ru/SiO_2 sample. It has been shown that incident light can couple into resonant photonic modes that propagate along films deposited on PC surfaces. These photonic modes extend the path-length and residence time of light within the film, thereby increasing absorption.[51–54] Since Ru/i-Si-o absorbs more strongly than Ru/SiO_2-o, it will be heated to a greater extent, thereby accelerating the Sabatier reaction *via* a photothermal effect. For a blank test, ran under high light intensities and without a sample in the reactor, the temperature inside the reactor increased from ambient temperatures to almost 50 °C over a two hour period (Fig. S2, ESI†). Furthermore, the temperature of the back-side of the silicon wafers the PC supports were deposited on increased to ~150 °C during the photomethanation tests for both the Ru/i-Si-o and Ru/SiO_2-o samples. However, it has been shown that under intense illumination localized temperatures on metallic nanostructured photocatalysts can be elevated by several hundred degrees.[55–57] Thus, it is expected that the temperature of the Ru film residing on the PC supports under intense solar-simulated radiation is elevated to temperatures significantly higher than 150 °C. That is, interband absorption occurring in the Ru film will increase its temperature *via* a photothermal effect.[58,59] This photothermal heating may cause localized "hot-spots" on the PC-supported Ru film that increase the photomethanation rate at nearby active catalytic sites. Moreover, the i-Si-o support may provide an additional source of photothermal heating. Energy from light absorption in the i-Si-o support may generate thermal energy that transfers to the Ru film residing on its surface.

A photothermal effect may also be considered by comparing photomethanation rates for measurements performed at equal incident light intensities but different incident light spectra. That is, for tests performed at comparable incident light intensities photomethanation rates were greater when no filter was used as compared to the case when a 495 nm cut-off filter was used. For example, at incident light intensities of about 900 mW cm^{-2} photomethanation rates over the Ru/i-Si-o sample is 0.57 mmol g^{-1} h^{-1} when the cut-off filter is used and 1.44 mmol g^{-1} h^{-1} when the test is performed without a filter. Also, the photomethanation rate over the Ru/SiO_2-o sample is 0.058 mmol g^{-1} h^{-1} when the cut-off filter is used and 0.54 mmol g^{-1} h^{-1} when the test is performed without a filter. These results show that for an equal light intensity of about 900 mW cm^{-2} an incident light spectrum with a greater distribution of higher energy photons yields larger photomethanation rates as compared to a spectrum with a higher distribution of low energy photons. As these results are observed over both the Ru/i-Si-o and Ru/SiO_2-o samples we attribute this to a photothermal effect whereby, on a per energy basis, higher energy phonons generated from the absorption of higher energy photons accelerate the methanation reaction to a greater extent than lower energy phonons.

Moreover, the photomethanation rates for tests performed with or without a cut-off filter at incident light intensities of 900 mW cm^{-2} or greater exceeded methanation rates measured for tests carried out in the dark at 150 °C. Also, for the photomethanation tests performed without a filter, as the incident light intensity is increased from 900 mW cm^{-2} to 1720 mW cm^{-2} and 2470 mW cm^{-2} the photomethanation rates continue to rise, although this rate increase is not linear and the amount of CH_4 produced per incident light power exhibits a slight downward trend. As the incident light intensity increases the temperature difference between the sample and its surroundings increases, and a greater portion of the photothermal energy generated in the sample is lost to the surrounding reactant and product gases and reactor walls.

For a photochemical effect to occur photo-generated charge carriers would have to transfer form the i-Si-o support to the Ru catalyst and participate in the photomethanation reaction. It is possible for photo-excited charge carriers to transfer from the i-Si-o support to the Ru film as the work function of Ru metal and the fermi level of intrinsic Si has been reported to be ~4.7 eV and ~4.75 eV, respectively.[60,61] However, the electron and hole lifetimes in the i-Si-o support are expected to be on the order of ~100 ns or less,[62] and it is expected that the vast

majority of photo-excited charge carriers generated in the i-Si-o support will immediately recombine and generate phonons that transfer across the Ru/i-Si-o interface to provide heat at catalytic sites on the surface of the Ru film. In comparison, the SiO_2-o support is not highly absorbing and therefor is not expected to provide photothermal heating to the same extent as the i-Si-o support.

We also performed DFT analysis to further investigate how photo-induced charges might enhance the Sabatier reaction. The vast majority of photogenerated charge carriers in the Ru/SiO_2 and Ru/i-Si-o samples will recombine on timescales much shorter than those required to perform photochemistry, however, residual photogenerated charges in trap states and surface states may induce charges on the Ru surface that can facilitate the Sabatier reaction.[63] It has been proposed in the literature that CO_2 hydrogenation on Ru surfaces proceeds with the formation of an HCOO intermediate which dissociates into O and CHO, which further dissociates to C or CH species, subsequently undergoing a series of hydrogenation steps before forming CH_4.[64] It has also been reported in the literature that in the first step of the Sabatier reaction CO_2 readily dissociates to adsorbed CO and O on the Ru surface, which are then hydrogenated.[65–67] Regardless of the reaction intermediates and mechanisms, it is generally accepted that the reaction rate is limited by the number of active surface Ru–H bonds. To investigate how surface charge effects the Sabatier reaction rate over Ru, we performed DFT calculations on the low-index Ru(0001) surface. This surface is modeled as a 6-layer slab comprised of 54 atoms, separated from periodic images by a 20 Å thick vacuum layer. The slab is periodic along directions parallel to the surface, and is sandwiched by a semi-infinite effective screening medium (ESM) representing a vacuum in both directions normal to the surface. The modeled system is a continuous layer, 10.7 Å in thickness, which represents a Ru nanofilm, and captures the behavior of non-edge nanocrystal regions which form the majority of the surface area. In order to investigate the catalytic effects of surface charge on the supported Ru surface, we also modelled the Ru(0001) surface with one extra electron ($[Ru(0001)]^{-1}$) and with one less electron ($[Ru(0001)]^{+1}$). We then analyzed the interaction between the [Ru(0001)], $[Ru(0001)]^{-1}$ and $[Ru(0001)]^{+1}$ surfaces with the reactant and product gases (CO_2, H_2, H_2O and CH_4), as discussed below.

First we analyzed adsorption of the CO_2 molecule on the neutral and charged Ru(0001) surfaces. The optimized geometries of CO_2 adsorbed [Ru(0001)], $[Ru(0001)]^{-}$ and $[Ru(0001)]^{+}$ surfaces are shown in Fig. 4(a–c). The CO_2 molecule, initially placed in the vicinity of the Ru surface atoms for all cases, did not show any interaction with the $[Ru(0001)]^{+1}$ surface and remained intact, moving about 2.4 Å away during optimization (Fig. 4(c)). However, CO_2 was adsorbed on the [Ru(0001)] and $[Ru(0001)]^{-1}$ surfaces by bending and forming a C–Ru bond (Fig. 4(a and b)). On the [Ru(0001)] surface the C–O bond lengths within the CO_2 molecule increases from 1.16 Å to 1.21 Å and 1.35 Å, and the bond angle decreases from 180° to 128°, whereas on the $[Ru(0001)]^{-1}$ surface, the C–O bond lengths increase to 1.25 Å and 1.27 Å, while the bond angle decreases to 136°. The binding energy of the CO_2 molecule on the [Ru(0001)] and $[Ru(0001)]^{-1}$ surfaces is +0.00014 eV and +2.96 eV, respectively,

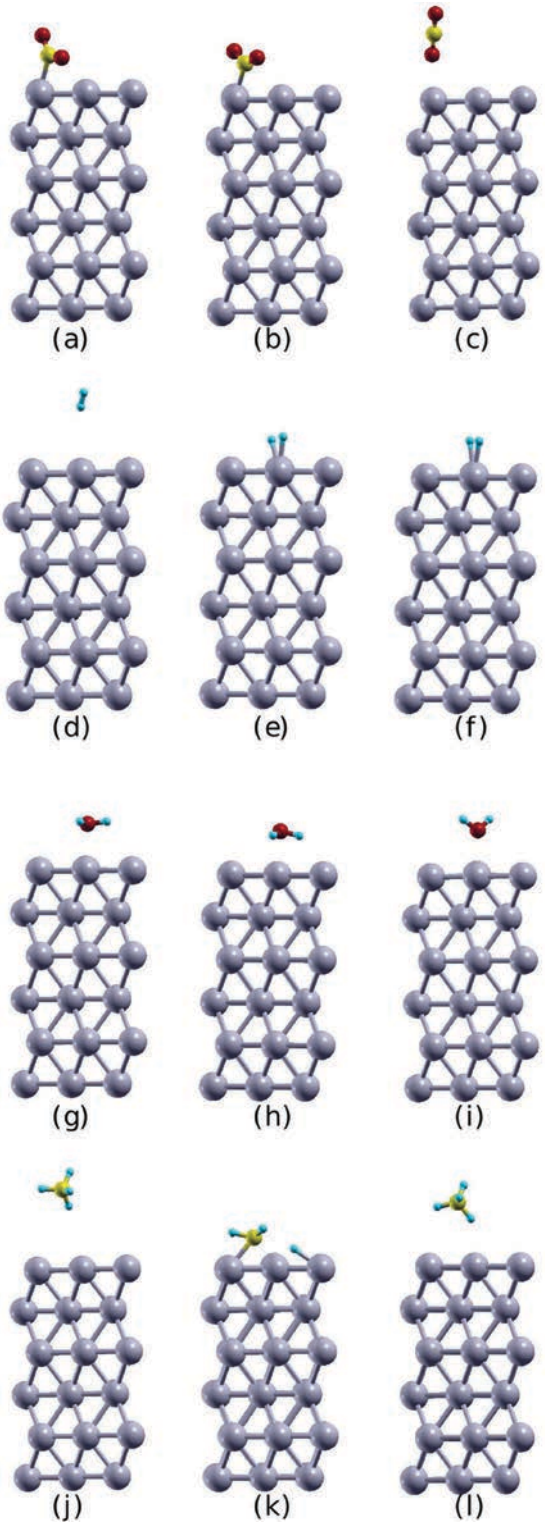

Fig. 4 The optimized geometries of adsorbed (a–c) CO_2, (d–f) H_2, (g–i) H_2O, and (j–l) CH_4 on [Ru(0001)] (left), $[Ru(0001)]^{-1}$ (middle) and $[Ru(0001)]^{+1}$ (right) surfaces. The grey, blue, red and yellow spheres represent Ru, H, O and C atoms, respectively.

which suggests that CO_2 is relatively stable when adsorbed on the [Ru(0001)] surface, but is highly unstable and more likely to dissociate when adsorbed on the $[Ru(0001)]^{-1}$ surface.

To investigate the effects of the Ru(0001) surface charge on the adsorption of H_2, an individual H_2 molecule was positioned sufficiently far from the Ru surface (3 Å) at the onset of the DFT calculations, and the geometries are optimized (Fig. 4(d–f)). Then we performed Bader charge, bond length, and binding energy analyses on these optimized geometries (Table S1, ESI†).[68] Interestingly, results show that while the H_2 molecule remains intact after relaxation on the neutral [Ru(0001)] surface, it undergoes exothermic homolytic splitting on the charged $[Ru(0001)]^{-1}$ and $[Ru(0001)]^{+1}$ surfaces. This homolytic dissociative adsorption of H_2 on charged Ru surfaces can be understood in terms of a model where H_2 donates σ-orbital bonding electrons to the positively charged Ru surface or H_2 accepts σ*-orbital antibonding electrons from the negatively charged Ru surface, both effects serving to weaken and enable homolytic dissociation of adsorbed H_2 on the Ru surface.

To further understand the charge distribution we conducted charge density difference (CDD) analysis for H_2 adsorption on [Ru(0001)], $[Ru(0001)]^{-1}$ and $[Ru(0001)]^{+1}$ surfaces as shown in Fig. 5(a), (b) and (c), respectively. As shown in Fig. 5(a), there is only a slight interaction between H_2 and the neutral Ru(0001) surface, suggesting that hydrogen binds by a weak electrostatic dipole mechanism with the neutral surface. However, H_2 adsorption on the charged Ru surfaces leads to a reduction in charge density between the two H atoms and an increase in charge density between the hydrogen atoms and the Ru surfaces (Fig. 5(b and c)) showing dissociative chemisorption of the H_2 molecule. Moreover, the negative charge on chemisorbed hydrogen calculated from Bader charge analysis (Table S1, ESI†), shows that irrespective of the nature of charge on the surfaces, hydrogen splits and becomes chemisorbed on the charged surfaces as a hydride.

We also conducted DFT analysis to explore the interaction between the Sabatier reaction products, H_2O and CH_4, with the neutral [Ru(0001)] and charged, $[Ru(0001)^{\pm1}]$ surfaces by placing H_2O and CH_4 in the vicinity of the surface Ru atoms. The optimized geometries show that H_2O in the ground state does not interact with any of the [Ru(0001)], $[Ru(0001)^{+1}]$, or $[Ru(0001)^{-1}]$ surfaces. Instead, the H_2O atom moves about 2.3 Å, away from all surfaces during relaxation, keeping its geometry unaltered (Fig. 4(g–i)). However, it should be noted that the $[Ru(0001)]^{+1}$ and $[Ru(0001)]^{-1}$ surfaces do exhibit a weak interaction with the O and H atoms of H_2O, respectively, which might hinder H_2O desorption, slowing the Sabatier reaction rate. Further, the CH_4 adsorption analysis shows that at ground state the CH_4 molecule does not interact, but moves 4.2 Å and 3.4 Å away from the neutral [Ru(0001)] and charged $[Ru(0001)^{+1}]$ surfaces, as shown in Fig. 4(j) and (l), respectively. However, as shown in Fig. 4(k), CH_4 is highly unstable on the $[Ru(0001)]^{-1}$ surface and dissociates into CH_3 and H, which suggests that it will be difficult to desorb CH_4 from the $[Ru(0001)]^{-1}$ surface.

The results from the DFT analysis suggest that both positive and negative charge residing on the Ru surface may accelerate the Sabatier reaction. However, it is expected that the $[Ru(0001)]^{-1}$ surface is likely the most active towards the Sabatier reaction because the CO_2 molecule bends on the $[Ru(0001)]^{-1}$ surface, and the bent CO_2 molecule is highly unstable and may readily react on this surface. Also, most importantly, H_2 adsorbs and dissociates on the $[Ru(0001)]^{-1}$ surface such that it can readily react with the adsorbed CO_2 molecule. It is noteworthy that XPS measurements taken on the Ru/i-Si-o sample before and after the Sabatier reaction rate measurements were performed, revealed that the Ru film on the i-Si-o sample becomes highly reduced under reaction conditions (Fig. S3, ESI†). This highly reduced state may be induced by the hydrogen environment during reaction conditions and/or by photo-excited electrons. This highly reduced state may also contribute to the formation of Ru–H surface bonds and the reduction of adsorbed CO_2.

Experimental

Fabrication of the photonic crystal supports

SiO_2 spheres with a diameter of ~460 nm were synthesized using a modified Stöber process and subsequently crystallized

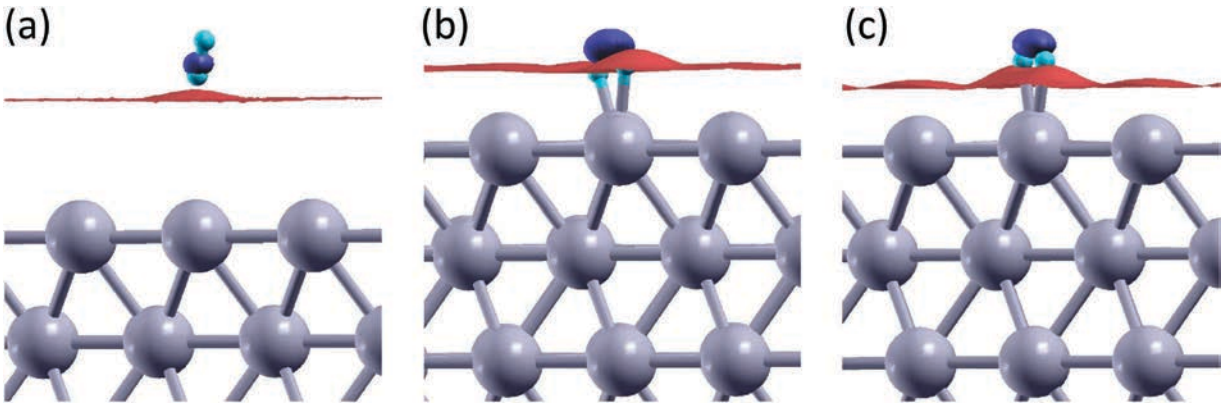

Fig. 5 Charge density difference isosurfaces for H_2 adsorption on [Ru(0001)], $[Ru(0001)]^{-1}$, and $[Ru(0001)]^{+1}$ surfaces, respectively (a–c). Blue indicates regions of charge loss and red indicates regions of charge gain. Grey and blue spheres represent Ru and H atoms, respectively.

as SiO_2-o films using the evaporation-induced self-assembly (EISA) method on a polished silicon wafer with a surface area of approximately 1 cm × 2 cm. The i-Si-o film was fabricated by infiltrating the interstitial voids in these SiO_2-o films with amorphous silicon using a home-built dynamic chemical vapour deposition (CVD) apparatus and subsequently removing the SiO_2-o template by etching them in a solution containing HF. The attained i-Si-o films were then crystallized by subjecting them to an annealing treatment at a temperature of 630 °C for a duration of 5 h.

Catalyst loading

The 50 nm thick Ru film was deposited on top of the SiO_2-o and i-Si-o supports in a custom-built sputtering system (Kurt J. Lesker Co.) by radio frequency (RF) magnetron sputtering using a 99.95% pure Ru sputtering target purchased from Angstrom Sciences, Inc. The base pressure of the sputtering chamber was pumped down to 1×10^{-7} Torr before argon was introduced into the chamber at a flow rate of 20 sccm. The chamber pressure, discharge power and substrate-to-target distance was set to 3 mTorr, 100 W and 14 cm, respectively. The sputtering process was terminated when 50 nm of Ru, as measured from an *in situ* thickness monitor (SQM-242 from Sigma), had been deposited.

Sample characterization

Optical measurements were performed with a UV/Vis/NIR spectrometer (Perkin-Elmer Lambda 1050) equipped with an integrating sphere. The absorption for each sample was estimated using the equation $\%A = 100 - (\%T + \%R)$ where $\%R$ and $\%T$ are the diffuse reflectance and transmittance, respectively. SEM images were taken using a Hitachi S-5200 high-resolution scanning electron microscope. X-ray photoelectron spectroscopy (XPS) measurements were performed in an ultrahigh vacuum chamber with a base pressure of 10^{-9} Torr. The system used a Thermo Scientific K-Alpha XPS spectrometer, with an Al K_α X-ray source operating at 12 kV, 6 A and X-ray wavelengths of 1486.7 eV. The spectra were obtained with an analyzer pass energy of 50 eV with energy spacing of 0.1 eV. All data analysis was carried out using Thermo Scientific Avantage software.

Sabatier reaction rate measurements

Gas-phase photocatalytic rate measurements were conducted in a custom-built 12 mL stainless steel batch reactor with a fused silica view port sealed with Viton O-rings (Fig. S5, ESI†). The pressure inside the reactor was monitored using an Omega PX309 pressure transducer. The duration of all runs was 2 h. Product gases were analyzed with a flame ionization detector (FID) and thermal conductivity detector (TCD) installed in a SRI-8610 Gas Chromatograph (GC) with a 3′ Mole Sieve 13a and 6′ Haysep D column. For heated tests the reactor temperature was controlled by an OMEGA temperature controller combined with a thermocouple placed in contact with the rear side of the sample. The reactor was heated to 150 °C and purged with H_2 for twenty minutes prior to being infiltrated with CO_2 and H_2 at a $H_2:CO_2$ ratio of 4:1. For tests wherein the sample was irradiated with light the lamp was turned on once the reactor valves were closed. The spectral output was measured using a StellarNet Inc. spectrophotometer and the power of the incident irradiation was measured using a Spectra-Physics power meter (model 407A).

Computational details

DFT calculations were carried out using Quantum ESPRESSO code, PWSCF package.[69] The plane-wave-pseudopotential approach, together with the Perdew–Burke–Ernzerhof (PBE) exchange–correlation functional, and Vanderbilt ultrasoft pseudopotentials was utilized throughout the analysis.[69–71] All calculations are non-spin polarized. The kinetic energy cut-offs of 40 and 160 Ry were used for the smooth part of the electronic wavefunctions and augmented electron density, respectively. The self-consistent field convergence criterion was set to 1×10^{-6} Ry per Bohr and the structures were relaxed using a conjugate gradient minimization algorithm until the magnitude of the residual Hellmann–Feynman force on each surface atom was less than 10^{-3} Ry per Bohr. Brillouin zone integrations were performed using a Monkhorst–Pack grid of 4 × 4 × 1 k points.[72] The binding energy was calculated using the following equation:

$$E_b = \left[E_{Ru(0001)+nH_2} - \left(E_{Ru(0001)} + nE_{H_2}\right)\right]/n$$

where $E_{Ru(0001)+nH_2}$ is the total energy of the neutral or charged Ru(0001) surface adsorbed with hydrogen, $E_{Ru(0001)}$ is the total energy of the neutral or charged Ru surface, E_{H_2} is the total energy of the free H_2 molecule and n corresponds to the number of H_2 molecules. A negative binding energy indicates a stable system configuration whereas a positive binding energy indicates an unstable system configuration.

Conclusions

In this work we investigated and compared Sabatier reaction rates over Ru films sputtered onto silica opal and inverted silicon opal photonic crystal supports at ambient temperature under solar simulated radiation as a function of incident illumination intensity. The largest rate observed in this study was 2.8 mmol g^{-1} h^{-1}, which was measured over the Ru/i-Si-o sample under high-intensity solar-simulated light at an intensity of 2470 mW cm^{-2}. Furthermore, photomethanation rates are roughly an order of magnitude larger when the Ru/SiO_2 and Ru/i-Si-o samples were tested under high-intensity solar-simulated light at an intensity of 2470 mW cm^{-2} as compared to rates measured in the dark at a temperature of 150 °C. However, the highest QE value for the tests performed in this work is $\sim 3 \times 10^{-4}$. This QE value was measured over Ru films on PC supports designed to investigate the photomethanation reaction, and with further understanding of photomethanation reaction mechanisms this value can be boosted by designing catalysts with a high density of photothermally activated sites that are accessible to high intensity incident radiation. This can be accomplished through the structural, compositional, optical and photonic materials engineering of hierarchical porous catalytic architectures, as

well as high-performance photoreactors that enable enhanced light harvesting with quantum efficiencies targeting technologically practical ranges of $>10\%$.

Moreover, for all reaction conditions methanation rates over the Ru/i-Si-o sample were significantly higher than that over the Ru/SiO_2 sample. We attribute the enhanced photomethanation rates over the Ru/i-Si-o sample to a photothermal effect caused by high absorption in the Ru/i-Si-o sample, wherein absorbed light energy is converted to heat. Furthermore, we performed DFT analysis to investigate whether photo-induced charges could also contribute to enhanced methanation rates over the PC supported Ru catalysts, which showed that H_2 has a stronger interaction with charged $[Ru(0001)]^{\pm1}$ surfaces. Specifically, H_2 homolytically dissociates and chemisorbs, forming Ru–H bonds on both negatively and positively charged Ru surfaces. A high density of H on the Ru surface will enhance the Sabatier reaction because, as commonly reported in the literature, the rate determining step is the hydrogenation of adsorbed CO_2. The results from the DFT analysis also showed that the CO_2 molecule bends when adsorbed on the negatively charged $[Ru(0001)]^{-1}$ surface; the bent CO_2 molecule is highly unstable and thus the Sabatier reaction may be accelerated on the $[Ru(0001)]^{-1}$ surface.

The work presented in this study illustrates the importance of the support material for photocatalysts. The open framework of the i-Si-o, with pores having a diameter on the scale of hundreds of nanometers, may prove to be highly advantageous in the design of high-throughput gas phase catalysts that convert CO_2 to CH_4 under high intensity illumination running at ambient temperatures. Also, the ability to reduce CO_2 at ambient temperatures by irradiating catalysts with high light intensity rather than heating the catalyst may procure numerous advantages. For example, lower operating temperatures may reduce heating loads and sintering, poisoning, mechanical degradation and eventual deactivation of the catalyst.

Conflicts of interest

The authors have no conflicts of interest to declare.

Acknowledgements

PGO and KKG contributed equally to this work. GAO is Government of Canada Research Chair in Materials Chemistry and Nanochemistry. Financial support for this work was provided by the Ontario Ministry of Research Innovation (MRI); Ministry of Economic Development, Employment and Infrastructure (MEDI); Ministry of the Environment and Climate Change; Connaught Innovation Fund; Connaught Global Challenge Fund; Natural Sciences and Engineering Research Council of Canada (NSERC). CVS acknowledges additional support from Compute Canada facilities ScieNet and Calcul Quebec, which enabled DFT simulations reported in this study. Dr Suezaki's assistance with sample preparation is greatly appreciated. We thank Dr Brodersen from the Ontario Centre for the Characterisation of Advanced Materials (OCCAM) for assistance with the XPS measurements. Chenxi Qian's assistance in preparing the TOC graphic is much appreciated.

Notes and references

1 M. Meinshausen, N. Meinshausen, W. Hare, S. C. B. Raper, K. Frieler, R. Knutti, D. J. Frame and M. R. Allen, *Nature*, 2009, **459**, 929.
2 B. W. Griscom, J. Adams, P. W. Ellis, R. A. Houghton, G. Lomax, D. A. Miteva, W. H. Schlesinger, D. Shoch, J. V. Siikamäki, P. Smith, P. Woodbury, C. Zganjar, A. Blackman, J. Campari, R. T. Conant, C. Delgado, P. Elias, T. Gopalakrishna, M. R. Hamsik, M. Herrero, J. Kiesecker, E. Landis, L. Laestadius, S. M. Leavitt, S. Minnemeyer, S. Polasky, P. Potapov, F. E. Putz, J. Sanderman, M. Silvius, E. Wollenberg and J. Fargione, *Proc. Natl. Acad. Sci. U. S. A.*, 2017, **114**, 11645.
3 C. Pasten and J. C. Santamarina, *Energy Policy*, 2012, **49**, 468.
4 S. N. Habisreutinger, L. S. Mende and J. K. Stolarczyk, *Angew. Chem., Int. Ed.*, 2013, **52**, 7372.
5 K. J. Kroeker, R. L. Kordas, R. Crim, I. E. Hendriks, L. Ramajo, G. S. Singh, C. M. Duarte and J.-P. Gattuso, *GCB Bioenergy*, 2013, **19**, 1884.
6 W. Tu, Y. Zhou and Z. Zhou, *Adv. Mater.*, 2014, **26**, 4607.
7 M. Aresta, in *Carbon Dioxide as Chemical Feedstock*, ed. M. Aresta, Wiley-VCH, Weinheim, 2010.
8 A. Dibenedetto, A. Angelini and P. Stufano, *J. Chem. Technol. Biotechnol.*, 2014, **89**, 334.
9 Q. Chen, M. Lv, Z. Tang, H. Wang, W. Wei and Y. Sun, *J CO_2 Util.*, 2016, **14**, 1.
10 R. J. Detz, J. N. H. Reek and B. C. C. van der Zwaan, *Energy Environ. Sci.*, 2018, **11**, 1653.
11 L. Yuan and Y.-J. Xu, *Appl. Surf. Sci.*, 2015, **342**, 154.
12 Y. Izumi, *Coord. Chem. Rev.*, 2013, **257**, 171.
13 Y. Izumi, *Recent Advances (2012–2015) in the photocatalytic conversion of carbon dioxide to fuels using solar energy: feseability for a new energy, Adv. CO_2 Capture, Sequestration Convers,* American Chemical Society, Washington, 2015, p. 46.
14 K. Li, B. Peng and T. Peng, *ACS Catal.*, 2016, **6**, 7485.
15 G. A. Olah, G. K. S. Prakash and A. Goeppert, *J. Am. Chem. Soc.*, 2011, **133**, 12881.
16 J. Gao, Q. Liu, B. Liu, Z. Zhong and F. Su, *RSC Adv.*, 2015, **5**, 22759.
17 P. J. Lunde and F. L. Kester, *J. Catal.*, 1973, **30**, 423.
18 C. C. Yang, J. Vernimmen, V. Meynen, P. Cool and M. Guido, *J. Catal.*, 2011, **284**, 1.
19 F. Sastre, A. Corma and H. García, *J. Am. Chem. Soc.*, 2012, **134**, 14137.
20 N. M. Gupta, C. S. Kamble, R. M. Iyer, K. R. Thampi and M. Gratzel, *Catal. Lett.*, 1993, **21**, 245.
21 F. W. Chang, M. S. Kuo, M. T. Tsay and M. C. Hsieh, *Appl. Catal., A*, 2003, **247**, 309.
22 Y. Zhao, B. Zhao, J. Liu, G. Chen, R. Gao, S. Yao, M. Li, Q. Zhang, L. Gu, J. Xie, X. Wen, L.-Z. Wu, C.-H. Tung, D. Ma and T. Zhang, *Angew. Chem., Int. Ed.*, 2016, **55**, 4215.

23 J.-N. Park and E. W. McFarland, *J. Catal.*, 2009, **266**, 92.
24 M. Tahir and N. S. Amin, *Appl. Catal., A*, 2015, **493**, 90.
25 C. C. Lo, C. H. Hung, C. S. Yuan and J. F. Wu, *Sol. Energy Mater. Sol. Cells*, 2007, **91**, 1765.
26 D. Saliba, A. Ezzeddine, R. Sougrat, N. M. Khashab, M. Hmadeh and M. Al-Ghoul, *Chem. Sus. Chem.*, 2016, **9**, 1.
27 K. R. Thampi, J. Kiwi and M. Grätzel, *Nature*, 1987, **327**, 506.
28 C. Revilliod, J. A. McEvoy and M. Grätzel, *Sol. Energy Mater.*, 1991, **24**, 522.
29 J. Melsheimer, W. Guo, D. Ziegler, M. Wesemann and R. Schlögl, *Catal. Lett.*, 1991, **11**, 157.
30 X. Meng, T. Wang, L. Liu, S. Ouyang, P. Li, H. Hu, T. Kako, H. Iwai, A. Tanaka and J. Ye, *Angew. Chem.*, 2014, **126**, 11662.
31 L. Zhu, M. Gao, C. K. N. Peh and G. W. Ho, *Mater. Horiz.*, 2018, **5**, 323.
32 F. Sastre, A. V. Puga, L. Liu, A. Corma and H. García, *J. Am. Chem. Soc.*, 2014, **136**, 6798.
33 P. G. O'Brien, A. Sandhel, T. E. Wood, A. A. Jelle, L. B. Hoch, D. D. Perovic, C. A. Mims and G. A. Ozin, *Adv. Sci.*, 2014, **1**, 1.
34 L. B. Hoch, P. G. O'Brien, A. A. Jelle, A. Sandhel, D. D. Perovic, C. A. Mims and G. A. Ozin, *ACS Nano*, 2016, **10**, 9017.
35 A. A. Jelle, K. K. Ghuman, P. G. O'Brien, M. Hmadeh, A. Sandhel, D. D. Perovic, C. V. Singh, C. A. Mims and G. A. Ozin, *Adv. Energy Mater.*, 2018, 1702277.
36 A. Blanco, E. Chomski, S. Grabtchak, M. Ibisate, S. John, S. W. Leonard, C. Lopez, F. Meseguer, H. Miguez, J. P. Mondia, G. A. Ozin, O. Toader and H. M. van Driel, *Nature*, 2000, **405**, 437.
37 S. John, *Phys. Rev. Lett.*, 1987, **58**, 2486.
38 E. Yablonovitch, *Phys. Rev. Lett.*, 1987, **58**, 2059.
39 J. D. Joannopoulos, S. G. Johnson, R. D. Meade and J. N. Winn, *Photonic Crystals: Molding the Flow of Light*, Princeton University Press, Princeton, NJ, 2nd edn, 2008.
40 M. Curti, J. Schneider, D. W. Bahnemann and C. B. Mendive, *J. Phys. Chem. Lett.*, 2015, **6**, 3903.
41 Q. Yang, M. Li, J. Liu, W. Shen, C. Ye, X. Shi, L. Jiang and Y. Song, *J. Mater. Chem. A*, 2013, **1**, 541.
42 Y. Li, T. Kunitake and S. Fujikawa, *J. Phys. Chem. B*, 2006, **110**, 13000.
43 M. Ren, R. Ravikrishna and K. T. Valsaraj, *Environ. Sci. Technol.*, 2006, **40**, 7029.
44 M. Shao, L. Cheng, X. Zhang, D. D. D. Ma and S. T. Lee, *J. Am. Chem. Soc.*, 2009, **131**, 17738.
45 Z. Kang, C. H. A. Tsang, N. B. Wong, Z. Zhang and S. T. Lee, *J. Am. Chem. Soc.*, 2007, **129**, 12090.
46 N. Megouda, Y. Cofininier, S. Szunerits, T. Hadjersi, O. ElKechai and R. Boukherroub, *Chem. Commun.*, 2011, **47**, 991.
47 T. Suezaki, P. G. O'Brien, J. I. L. Chen, E. Loso, N. P. Kherani and G. A. Ozin, *Adv. Mater.*, 2009, **21**, 559.
48 K. Ogura, M. Kawano and D. Adachi, *J. Mol. Catal.*, 1992, **72**, 173.
49 S. J. Tauster, *Acc. Chem. Res.*, 1987, **20**, 389.
50 S. Sciré, C. Crisafulli, R. Maggiore, S. Minicò and S. Galvagno, *Catal. Lett.*, 1998, **51**, 41.
51 P. G. O'Brien, N. P. Kherani, S. Zukotynsky, G. A. Ozin, E. Vekris, N. Tetreault, A. Chutinan, S. John, A. Mihi and H. Miguez, *Adv. Mater.*, 2007, **19**, 4177.
52 P. G. O'Brien, N. P. Kherani, A. Chutinan, G. A. Ozin, S. John and S. Zukotynski, *Adv. Mater.*, 2008, **20**, 1577.
53 A. Chutinan and S. John, *Phys. Rev. A: At., Mol., Opt. Phys.*, 2008, **78**, 023825.
54 Y. Park, E. Drouard, O. El Daif, X. Letarte, P. Viktorovitch, A. Fave, A. Kaminski, M. Lemiti and C. Seassal, *Opt. Express*, 2009, **17**, 14312.
55 J. Jia, P. G. O'Brien, L. He, Q. Qiao, T. Fei, L. M. Reyes, T. E. Burrow, Y. Dong, K. Liao, M. Varela, S. J. Pennycook, M. Hmadeh, A. S. Helmy, N. P. Kherani, D. D. Perovic and G. A. Ozin, *Adv. Sci.*, 2016, **3**, 1600189.
56 G. Baffou and R. Quidant, *Laser Photonics Rev.*, 2013, **7**, 171.
57 S. Linic, U. Aslam, C. Boerigter and M. Morabito, *Nat. Mater.*, 2015, **14**, 567.
58 E. Anno and T. Yamaguchi, *Phys. Rev. B: Condens. Matter Mater. Phys.*, 1997, **55**, 4783.
59 K. A. Kress and G. J. Lapeyre, *J. Opt. Soc. Am.*, 1970, **60**, 1681.
60 *CRC Handbook of Chemistry and Physics*, ed. D. R. Lide, CRC Press, Boca Raton, Fl, 2001, pp. 12–130.
61 A. Novikov, *Solid-State Electron.*, 2010, **554**, 8.
62 A. Sa'ar, Photoluminescence from silicon nanostructures, in *Handbook of Nanophysics*, ed. K. D. Sattler, CRC Press, 2010, ch. 25.
63 A. J. Cowan and J. R. Durrant, *Chem. Soc. Rev.*, 2013, **42**, 2281.
64 S. Zhang, H. Yan, M. Wei, D. G. Evans and X. Duan, *RSC Adv.*, 2014, **4**, 30241.
65 M. R. Prairie, A. Renken, J. G. HighField, K. R. Thampi and M. Grätzel, *J. Catal.*, 1991, **129**, 130.
66 S. Eckle, H. G. Anfang and R. J. Behm, *J. Phys. Chem. C*, 2011, **115**, 1361.
67 F. Solymosi, A. Erdöhelyi and M. J. Kocsis, *J. Chem. Soc., Faraday Trans. 1*, 1981, **77**, 1003.
68 F. W. Bader and P. J. MacDougall, *J. Am. Chem. Soc.*, 1985, **107**, 6788.
69 P. Giannozzi, S. Baroni, N. Bonini, M. Calandra, R. Car, C. Cavazzoni, D. Ceresoli, G. L. Chiarotti, M. Cococcioni, I. Dabo, A. Dal Corso, S. de Gironcoli, S. Fabris, G. Fratesi, R. Gebauer, U. Gerstmann, C. Gougoussis, A. Kokalj, M. Lazzeri, L. Martin-Samos, N. Marzari, F. Mauri, R. Mazzarello, S. Paolini, A. Pasquarello, L. Paulatto., C. Sbraccia, S. Scandolo, G. Schauzero, A. P. Seitsonen, A. Snogunov, P. Umari and R. M. Wentzcovitch, *J. Phys.: Condens. Matter*, 2009, **21**, 395502 (Quantum Espresso: a modular and open-source software project for quantum simulations of materials).
70 J. P. Perdew, K. Burke and M. Ernzerhof, *Phys. Rev. Lett.*, 1996, **77**, 3865.
71 D. Vanderbilt, *Phys. Rev. B: Condens. Matter Mater. Phys.*, 1990, **41**, 7892.
72 H. J. Monkhorst and J. D. Pack, *Phys. Rev. B: Condens. Matter Mater. Phys.*, 1976, **13**, 5188.